Journal of Rock Mechanics & Tunnelling Technology (JRMTT)
25 (1) 2019 pp 7-20

Available online at www.isrmtt.com

Three Dimensional Coupled Stress-Flow Analysis of Underground Excavations in Jointed Rock Masses

Moataz A. Al-Obaydi

College of Engineering, University of Mosul, Mosul, Iraq

*M.N.Viladkar**
N.K. Samadhiya

Indian Institute of Technology Roorkee, Roorkee-247 667, India

**E-mail of Corresponding Author: mnviladkar50@gmail.com*

ABSTRACT

Redistribution of stresses in jointed rock mass occurs as a result of creation of an underground excavation. This alteration in stress pattern leads to changes in porosity or void ratio of rock material as well as in the aperture, i.e. closure or opening of the rock joints. If the rock mass surrounding the excavation is in a saturated condition, realistic behavior of the excavation can be understood only when a coupled stress-flow analysis is carried out. The present study proposes a coupled three dimensional stress-flow analysis of an underground excavation relating the stress and flow characteristics by an indirect method. Opening or closure of joints due to normal and shear stresses has been considered with due attention to the dilatant nature of rough discontinuities. As a result, the aperture of joints alters causing a further change in the permeability of rock mass also. Joint properties including the attitude of joint, stiffness, aperture, spacing and the roughness have been taken into account in the derivation of the constitutive laws and the behavior of a tunnel excavated in jointed rock mass has been examined. More disturbances in the contours of hydraulic head and pore water pressure have been observed near the tunnel periphery. The change in permeability upon redistribution of stresses is a function of the opening/closure of the joints. It has also been shown that the orientation and aperture of the joints have a pronounced effect on the fluctuation of the phreatic surface.

Keywords: Jointed rock mass; Coupled stress-flow; Hydro-mechanical constitutive law; Finite element method.

1. INTRODUCTION

In geotechnical engineering problems, the effect of flow through fractured or porous media can be studied in terms of the effective stresses. Barton et al. (1985) developed a constitutive model which provides shear stress-displacement-dilation-conductivity coupling. Based on the concept of joint roughness coefficient, *JRC*, a shear-dilation model was established. The normal closure of joint aperture was expressed based on a hyperbolic model for loading and unloading. Elsworth and Goodman (1986) related the changes in hydraulic conductivity with induced deformation in fractured rock masses on the basis of their observations of saw tooth and sinusoidal fissured surfaces. Wei and Hudson (1988) related hydraulic aperture with the closing and opening of a joint in a jointed rock mass using a hyperbolic function. The variation in permeability appears to be correlated to the variation in normal stress in a major zone of granite boreholes (Martin et al., 1990). Ouyang and Elsworth (1993) proposed a model to represent the mechanics of enhancement

of hydraulic conductivity of fractured rock caused by deformation, through the use of a modulus reduction ratio, R_m. This ratio considers the expression of hydraulic conductivity to account for the influence of joint aperture, joint spacing, joint stiffness and modulus of intact rock on the change of conductivity. Barton et al. (1995) showed that interaction between the state of stress and the fracture characteristics is determined not only by the orientation of aperture and hydraulic conductivity of individual fractures but also by the magnitude and orientation of all the three-principal stresses. When faults are artificially stressed, increased permeability may cause a movement of fluid along the faults. Liao and Hencher (1997) demonstrated, through the use of UDEC that alteration of stress significantly controls the fluid flow along the fractures. This behavior depends upon fracture intensity, orientation, distribution, and the connectivity. The coupled stress-permeability relationship for anisotropic fractured porous rocks was proposed by Chen and Bai (1998). A strong stress-dependency of changes in permeability were observed in a three dimensional fractured network where fracture can be arbitrarily oriented. Observation of Esaki et al. (1999) also indicated that change of hydraulic conductivity within the joint is similar to that of its dilatancy. The hydraulic conductivity increases rapidly by about 1.2 to 1.6 order of magnitude for the first 5mm shear displacement, whereas in the residual range, it becomes approximately constant with increasing shear displacement. Olsson and Barton (2001) have conducted a hydro-mechanical direct shear test to couple the changes in mechanical aperture to the corresponding changes in hydraulic aperture. A cubic law for flow in rock and a steady laminar flow between smooth parallel plates through rock joint were adopted in the analysis. In the analysis of a tunnel at Chandni Chowk location of Delhi metro in India, Rao and Gopichand (2002) showed that both stresses and displacements increase with saturation level and thus the factor of safety decreases. The experimental findings of Jing and Hudson (2004) indicate that joint roughness is a decisive factor in all aspects of hydro-mechanical behavior of rock fractures. Conventional parallel shear-flow tests were found to be not adequate for representing the general stress-flow behavior of rock fractures. In the study of variation in permeability due to excavation, Wei and Hudson (1990) considered a fluid flow and Drucker–Prager criterion to represent the plastic yield function of a joint in the jointed rock mass. The change in permeability is caused around underground openings by stress redistribution which accompanies the excavation. The relation between permeability and the strain was cited as,

$$\kappa = \kappa_0 \, e^{-\beta \varepsilon} \tag{1}$$

where, κ is the permeability at a specified stage of excavation, κ_0 is the initial value of permeability, e is the aperture, $\beta = E\ \alpha$ where E is the modulus of elasticity, α denotes the empirical parameter, and ε represents the strain at a specified stage of excavation. Wang et al. (2009) tried to simulate the coupled problem of seepage and stress around an underground excavation through jointed rock mass considering the characteristics of flow through the joints using distinct element method. Amberg (2009) dealt with the effect of the groundwater and time on the behavior of tunnels in soft rocks to present a methodology for plotting the ground reaction curves. The simulation was two dimensional in nature. It points out the need of three dimensional simulation to account for simulating the complete sequence of excavation experiencing the seepage pressure. Prassetyo (2017) presented a novel and efficient sequential coupling technique for hydro-mechanical analysis of tunneling in a saturated ground. Zhao (2018) conducted direct shear tests and shear-flow coupled tests with different joint roughness, normal stresses, and seepage pressures to investigate the shear behavior of jointed rock, choosing saw tooth surface as a simplification of the natural structural planes. The mechanisms of shear strength, seepage process, and shear failure modes under different conditions were compared and evaluated. The results could improve the basis of work for studying the mechanics and hydraulic characteristics of jointed rock mass, thus providing application value for problems of underground excavations.

In the present study, a three dimensional coupled stress-flow analysis has been presented which relates the stress and flow by an indirect method. Mathematical formulation has been presented to express the coupled stress-flow problem for jointed rock masses.

2. INFLUENCE OF STRESSES ON HYDRAULIC CONDUCTIVITY

2.1 General

Redistribution of stresses in jointed rock mass occurs as a result of underground excavations or any other activity that alters the stresses in the region. This alteration in stress pattern contributes to the change in porosity or void ratio of rock material as well as the change in aperture, i.e. closure or opening of the rock joint. In this study, it has been assumed that there is no effect of stress changes on porosity or void ratio of the rock material. This actually is not a realistic assumption, though however, it has a small effect on the permeability of rock material. The permeability of intact rock material at zero stress level can be found from laboratory tests.

The permeability of rock joint is related to the aperture. As mentioned in literature, the aperture is a function of stresses acting on the joint plane and hence, the permeability is stress dependent. The effect of stress is negligible in the region remote from the excavation, i.e. when there is no change in stresses.

2.2 Constitutive Law for Coupled Stress-Flow in Jointed Rock Masses

The following steps have been followed to evaluate the effect of stresses on the hydraulic conductivity of jointed rock mass:

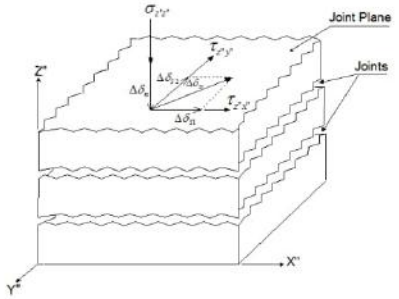

Fig. 1 – Displacements, normal and along the joint plane

i) The analysis of stress distribution in jointed rock mass is undertaken a- priory to evaluate the shear and normal stresses on the joint plane.

ii) Calculate the shear displacement, $\Delta\delta_s$ along the joint plane (local X″ Y″ plane in Fig. 1) using the equation,

$$\Delta\delta_s = \frac{\tau}{k_s} \tag{2}$$

in X"-direction, $\Delta\delta_{s1} = \frac{\tau_{z''x''}}{k_{s1}}$ (3a)

and in Y"-direction, $\Delta\delta_{s2} = \frac{\tau_{z''y''}}{k_{s2}}$ (3b)

where, $\Delta\delta_{s1}$ and $\Delta\delta_{s2}$ are respectively the shear displacements in X″ and Y″-directions (Fig. 1), $\tau_{z''x''}$ and $\tau_{z''y''}$ are the shear stresses acting on joint plane in X″ and Y″ directions, and k_{s1} and k_{s2} are respectively the values of shear stiffness of the joint in corresponding directions. The resultant shear displacement, $\Delta\delta_{sr}$ is,

$$\Delta\delta_{sr} = \left[\left(\Delta\delta_{s1} \right)^2 + \left(\Delta\delta_{s2} \right)^2 \right]^{1/2} \tag{4}$$

iii) Dilatant amount, Δδd is calculated as,

$$\Delta\delta_d = \Delta\delta_{sr} \tan(\beta) \tag{5}$$

where β is the dilatancy angle.

iv) The amount of joint closure, Δδn may be positive (joint opening) or negative (joint closure) depending upon the normal stress being either tensile or compressive and is calculated as -

$$\Delta\delta_n = \frac{\sigma_{z''z''}}{k_n} \tag{6}$$

where, $\sigma_{z''z''}$ is the normal stress on the joint plane, and k_n is the normal stiffness.

v) Finally, the aperture of joint, ē can therefore be defined as,

$$\bar{e} = e_0 + \Delta\delta_d \pm \Delta\delta_n \tag{7}$$

where, $\bar{e}$ is the adjusted value of joint aperture, e_0 is the initial value of aperture, $\Delta\delta_d$ is the dilatant amount, and $\Delta\delta_n$ is the normal displacement.

vi) The hydraulic conductivity of jointed rock mass, κj must be updated according to the adjusted value of aperture as,

$$\kappa_j = \frac{\gamma_w (\bar{e})^3}{12 \mu S_j R_c} \tag{8}$$

where, κ_j is the updated value of hydraulic conductivity, γ_w is the unit weight of water, μ is the dynamic viscosity of fluid i.e. water, S_j is the distance (spacing) between joints in one joint set, and R_c refers to the roughness coefficient factor.

vii) In matrix form, the hydraulic conductivity can be expressed as,

$$P_j'' = \begin{bmatrix} \kappa_{jx''} & 0 & 0 \\ 0 & \kappa_{jy''} & 0 \\ 0 & 0 & \kappa_{jz''} \end{bmatrix} \tag{9}$$

in which $\kappa_{jx''} = \kappa_{jy''} = \kappa_j$ (Eq. 9) while $\kappa_{jz''}$ represents the flow of water normal to the joint plane which depends on the conditions of flow.

viii) The hydraulic conductivity matrix can therefore be calculated and subsequently, the hydraulic head is evaluated at each nodal point of the domain by solving the equation system,

$$[H]\{\Phi\} = \{Q\} \tag{10}$$

where Φ represents hydraulic potential at any point. Thereafter, the pore water pressure, u is evaluated using the relations,

$$\{\phi_w\} = \{\Phi\} - \{h_z\} \tag{11}$$

in which h_z is the position or elevation head of the nodal point and

$$\{u\} = \{\phi_w\}\gamma_w \tag{12}$$

In this way, the stress effect is included in the present study.

2.3 Constitutive Laws of Coupled Stress-Flow along a Discontinuity

In order to evaluate the effect of stress on hydraulic conductivity of a major discontinuity, the procedure presented in previous article has been extended with the use of the following expression:

$$P_{dj} = \frac{\gamma_w \ (\bar{e})^2}{12\ \mu\ R_c} \tag{13}$$

After calculating the value of hydraulic conductivity based on the adjusted value of aperture, hydraulic conductivity matrix of the discontinuity can be calculated.

3. INTERACTION BETWEEN MECHANICAL BEHAVIOR AND PORE WATER PRESSURE IN JOINTED ROCK

The presence of water in rock mass leads to a change in the rock mass properties. In terms of effective stresses, the in-situ stresses can be written as,

$$\sigma'_{xo} = k_x \gamma H - u \tag{14a}$$
$$\sigma'_{yo} = k_y \gamma H - u \tag{14b}$$
$$\sigma'_{zo} = \gamma H - u \tag{14c}$$
$$\tau'_{xyo} = \tau_{xy} \tag{14d}$$
$$\tau'_{yzo} = \tau_{yz} \tag{14e}$$
$$\tau'_{zxo} = \tau_{zx} \tag{14f}$$

In matrix form,

$$\{\sigma'_o\} = \begin{Bmatrix} \sigma'_{xo} \\ \sigma'_{yo} \\ \sigma'_{zo} \\ \tau'_{xy} \\ \tau'_{yz} \\ \tau'_{zx} \end{Bmatrix} = \begin{Bmatrix} k_x \gamma Z - u \\ k_y \gamma Z - u \\ \gamma Z - u \\ \tau_{xy} \\ \tau_{yz} \\ \tau_{zx} \end{Bmatrix} \tag{15}$$

Similarly, the induced stresses can be represented using the effective stress concept as,

$$\{\sigma'\} = \begin{Bmatrix} \sigma'_x \\ \sigma'_y \\ \sigma'_z \\ \tau'_{xy} \\ \tau'_{yz} \\ \tau'_{zx} \end{Bmatrix} = \begin{Bmatrix} \sigma_x - u \\ \sigma_y - u \\ \sigma_z - u \\ \tau_{xy} \\ \tau_{yz} \\ \tau_{zx} \end{Bmatrix} \tag{16}$$

The effective principal stresses can be expressed as,

$$\{\sigma'_P\} = \begin{Bmatrix} \sigma'_1 \\ \sigma'_2 \\ \sigma'_3 \end{Bmatrix} = \begin{Bmatrix} \sigma_1 - u \\ \sigma_2 - u \\ \sigma_3 - u \end{Bmatrix} \tag{17}$$

The modulus of elasticity, E_r of rock material reduces due to the effect of pore water pressure. Normal stiffness and shear stiffness of the joint are also stress dependent. Therefore, their values change when effective stress concept is applied. Based on the effective stress concept, the compliance matrix is also affected by the presence of water through the change in the value of modulus of elasticity of the rock material and the stiffnesses of the joint.

4. COUPLED ANALYSIS OF TUNNEL THROUGH JOINTED ROCK MASS

4.1 Problem Definition

Analysis of a circular tunnel excavated in jointed rock mass, analyzed earlier by Wei and Hudson (1990), has been considered here for coupled stress-flow analysis. Figure 2 shows the geometric details of tunnel and the surrounding media. The tunnel has a diameter of 40 m and was excavated at a depth of 80 m below the ground surface. The length of tunnel considered for analysis is 200 m. The rock mass contains only one vertical joint set. Initially, the water table is located at a level of 65 m above the tunnel roof. The tunnel alignment has been assumed to be North-South. Three dimensional coupled stress–flow analysis of this tunnel has been carried out here using the finite element method so as to evaluate the effect of seepage flow on the resulting deformation and stress distribution around the tunnel. To accomplish this, three test runs have been carried out namely, seepage analysis, stress analysis and the coupled stress-flow analysis. The problem has been considered as an unconfined flow problem. This problem was analyzed earlier by Wei and Hudson (1990) using a 3D-FEM coupled stress-flow program. An empirical law given by Eq. 1 was used to describe the relation between permeability and the stress.

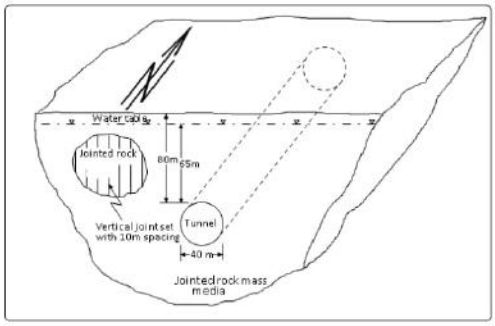

Fig. 2 – Geometry of circular tunnel excavated in jointed rock mass

The material properties for both the constituents of rock mass, i.e. rock material and rock joint considered for analysis have been presented in Table 1. Many parameters were not available in the literature (Wei and Hudson, 1990) and so suitable values have been assumed in the present study. These parameters include stiffness, aperture of the joint and unit weight of the rock mass. The joint permeability normal to the joint plane has been assumed to be 1×10^{-6} m/s.

Only in-situ stresses have been considered in the analysis. These have been considered as proportional to the height of overburden in the vertical direction and the corresponding lateral earth pressure in the horizontal direction. Accordingly, redistribution of stresses and their effect on hydraulic characteristics have been studied.

Table 1 - Material properties of rock mass surrounding the tunnel (after Wei and Hudson, 1990)

Material Type	S. No.	Material Properties	Symbol	Unit	Value
Rock Material	1	Modulus of elasticity	E	MPa	10000
	2	Poisson's ratio	ν	-	0.25
	3	Unit weight*	γ	kN/m^3	26.0
	4	Coefficient of lateral earth pressure at rest	k_o	--	0.40
	5	Initial Coefficient of permeability	κ_o	m/s	1×10^{-6}
Joint Set	6	Normal stiffness*	k_n	MPa/m	20000
	7	Shear stiffness*	k_s	MPa/m	2000
	8	Aperture*	e	mm	0.50
	9	Joint spacing	S_j	m	10.0
	10	Dip amount	α_j	Deg.	90
	11	Dip direction with tunnel axis	ω_j	Deg.	90

Only half of the domain of rock mass extending to 105 m along the width, 160 m along the height and 200 m along the length direction has been discretized as shown in Fig. 3. Finite element mesh consists of 760, 8-noded brick elements and 1110 nodes. The same mesh has been adopted both for seepage and the stress analysis.

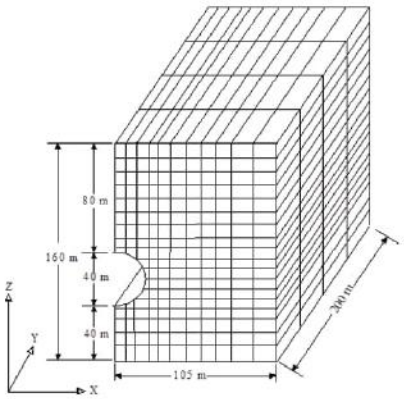

Fig. 3 – 3D-finite element mesh for half tunnel

4.2 Boundary Conditions

The analysis involves two algorithms, one for the stress analysis and the other for the seepage analysis.

i) *Stress analysis* – A restrained boundary condition has been imposed on all the nodes in the direction normal to the boundary planes except the top plane. The nodes around the periphery of the tunnel are left free to deform.

ii) Seepage analysis – This involves two types of boundary conditions:

a) Dirichlet boundary condition: an elevation head proportional to the elevation of a typical node on the periphery, has been applied on the nodes located along the periphery of the tunnel. For all the nodes on the right boundary plane, a hydrostatic head of 145 m has been applied.
b) Neumann boundary condition: the flow across the bottom most boundary has been defined as zero, i.e. no flow across the boundary condition.

4.3 Discussion of Results

4.3.1 Hydraulic characteristics

Contours of the hydraulic head causing the seepage and predicted on basis of the coupled stress-flow analysis have been presented in Fig. 4. As is obvious, the magnitude and distribution of hydraulic head changes due to the stresses in coupled (stress-flow analysis) and uncoupled (seepage analysis) conditions. Disturbances have been noticed in the flow pattern near the tunnel periphery in the region where there is significant stress redistribution. As such, a reduction in seepage head has been observed as one approaches the tunnel periphery. This may be due to the Dirichlet boundary condition of the elevation head imposed at the tunnel periphery.

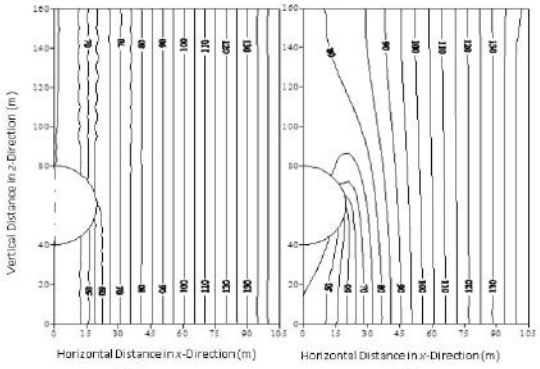

Fig. 4 – Contours of hydraulic head (m) around tunnel

Similarly, Fig. 5 shows changes in the pattern of pore water pressure distribution due to the redistribution of stresses. An increase in pore water pressure has been observed due to redistribution of stresses in the coupled stress-flow analysis. This is due to the reduction in permeability of the rock joints as a result of the closure of joints upon loading.

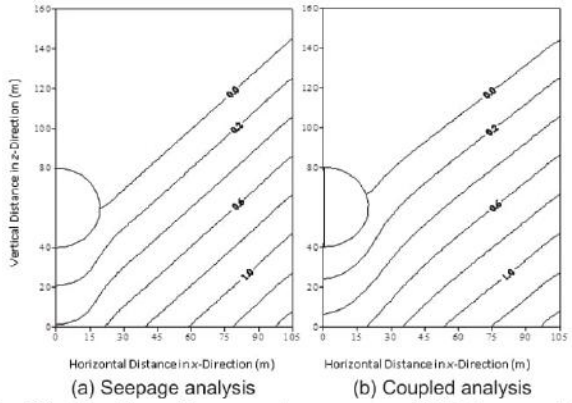

Fig. 5 – Distribution of pore water pressure (MPa) around tunnel

A comparison between the position of phreatic surface predicted in the present study and that reported by Wei and Hudson (1990) has been presented in Fig. 6. Despite some differences in both the studies, the overall trend remains the same. The difference is attributed to different constitutive laws adopted in the two studies. In addition, due to non-availability of some parameters in the study conducted by Wei and Hudson (1990), the difference can be attributed to values of various parameters assumed in the present study such as stiffness of the joint, aperture of the joint and unit weight of rock material which may be different from those used by Wei and Hudson (1990).

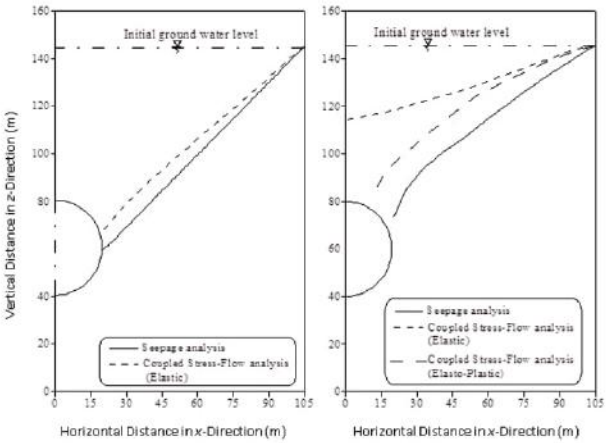

(a) Present study (b) After Wei and Hudson (1990)

Fig. 6 – Comparison of position of phreatic surface

4.3.2 Displacements

The variation of horizontal and vertical displacements obtained from both the coupled stress-flow and uncoupled analysis (stress analysis) of tunnel have been plotted as contours in Figs. 7 and 8 and compared with those for dry rock mass condition. It is clear that there are some changes in the magnitude of displacements in X and Z directions, although the pattern remains unchanged when the flow of water is considered. Displacements in Y direction are negligibly small for all practical purposes. There is a very small increase in displacement due to saturated condition. The contours suggest that at tunnel periphery, the displacement is inwards indicating the tunnel closure. Trajectory of contours of horizontal displacement, δ_x in the far away region is vertical.

The values of maximum displacements along the three reference directions at the crown, sidewalls and the invert of tunnel have been presented in Table 2. It appears that displacements remain practically unaffected by saturation. This may be attributed to the low water level over the roof of the tunnel and/or to the joint configuration, especially because there is only one joint set present and which is vertical. The maximum vertical displacements recorded at crown and the invert are respectively 5.36mm downward and 3.67mm upward. At the sidewall, horizontal displacement, δ_x and vertical displacement, δ_z are roughly equal and have caused the closure of tunnel.

Table 2 - Maximum displacement at the periphery of tunnel

Location	Displacement (mm) *					
	Stress Analysis			Coupled Stress-Flow analysis		
	δ_x	δ_y	δ_z	δ_x	δ_y	δ_z
Crown	0.00	-3×10^{-15}	-5.36	0.00	-2×10^{-6}	-5.46
Sidewall	-0.60	6×10^{-16}	-0.73	-0.62	-3×10^{-5}	-0.78
Invert	0.00	-3×10^{-16}	3.67	0.00	-7×10^{-6}	3.84

** δ_x: horizontal displacement in x-direction, δ_y: horizontal displacement in y-direction, δ_z: vertical displacement in z-direction*

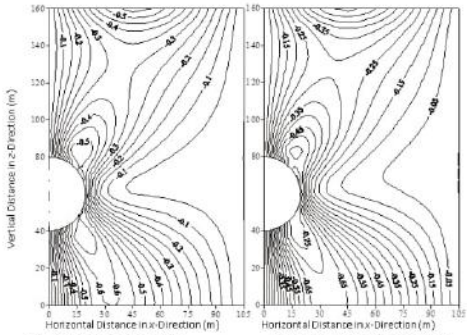

(a) Stress analysis (b) Coupled analysis

Fig. 7 – Contours of horizontal displacement, δ_x (mm) around tunnel

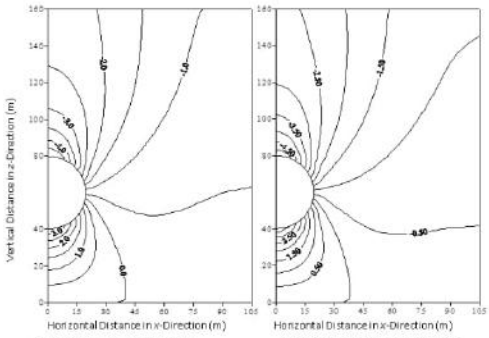

(a) Stress analysis (b) Coupled analysis

Fig. 8 – Contours of vertical displacement, δ_z (mm) around tunnel

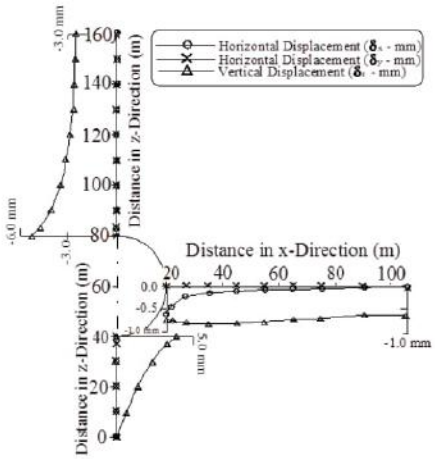

Fig. 9 – Variation of displacement along axes of tunnel mobilized

Figure 9 shows the variation of displacements along different axes of tunnel for saturated condition. Higher horizontal displacement, δ_x has been observed at the sidewall which becomes negligible at a distance of 80 m from tunnel periphery. The vertical displacement, δ_z is maximum both at tunnel crown and the invert and it decreases away from the tunnel periphery.

4.3.3 Stresses

i) The variation of effective stresses, σ'_x, σ'_y and σ'_z around the tunnel periphery has been plotted for both dry and saturated conditions in Figs. 10, 11 and 12 respectively. In the near field, the stresses show little variation while a perceptible change is visible in the far field. This depends upon the pore water pressure distribution.

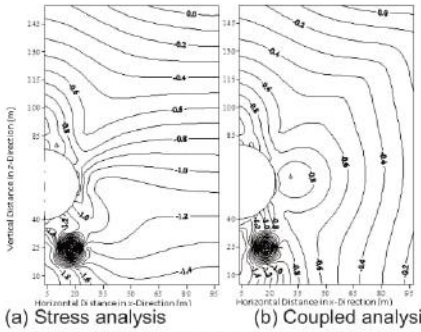

(a) Stress analysis (b) Coupled analysis

Fig. 10 – Contours of horizontal stress,σ_x (MPa) around tunnel

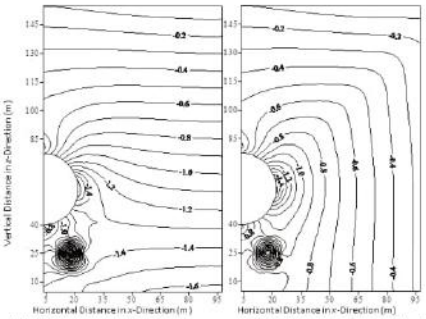

(a) Stress analysis (b) Coupled analysis

Fig. 11 – Contours of horizontal stress,σ_y (MPa) around tunnel

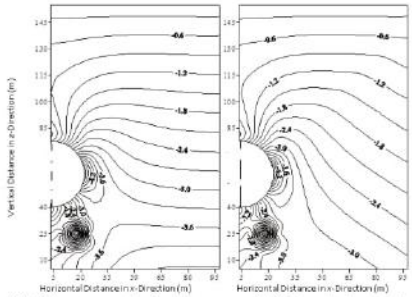

(a) Stress analysis (b) Coupled analysis

Fig. 12 – Contours of vertical stress,σ_z (MPa) around tunnel

ii) Most of the stresses are compressive in nature due to bi-axial in-situ stress field.

iii) Table 3 shows a maximum vertical compressive stress, σ_z in the sidewall of tunnel of 5.752 MPa for dry rock mass which gives a stress concentration factor of 2.15. In the coupled stress-flow analysis also, the vertical stress is of the same order. On the other hand, the horizontal stress, σ_y is of the order 1.701 MPa which is about 82 percent of the applied horizontal stress of 2.08 MPa. The horizontal stress, σ_x is of order 0.54 MPa only. Accordingly, the horizontal stress, σ_y is 3 times higher than the horizontal stress, σ_x. This brings forth the fact that the intermediate stress, σ_y cannot be ignored in the analysis of underground structures and therefore a three dimensional analysis is essential.

Table 3 - Average stresses at the periphery of tunnel

Location	Stresses* (MPa)					
	Stress Analysis			Coupled Stress-Flow Analysis		
	σ_x	σ_y	σ_z	σ'_x	σ'_y	σ'_z
Crown	-0.823	-0.352	-0.174	-0.827	-0.353	-0.175
Sidewall	-0.546	-1.701	-5.752	-0.532	-1.686	-5.744
Invert	-1.316	-0.547	-0.492	-1.296	-0.544	-0.301

σ_x: horizontal stress in x-direction, σ_y: horizontal stress in y-direction, σ_z: vertical stress in z-direction.

iv) The stresses obtained in coupled stress-flow analysis are comparable to those of stress analysis for dry condition. The stresses at invert of the tunnel are higher than those at the crown or in the sidewalls. Maximum effective vertical stresses at crown and invert are 0.175 MPa and 0.301 MPa respectively. The horizontal stress, σ_x is about 4 to 5 times the vertical stress at crown and invert. It is about 2 times the horizontal stress in Y direction, σ_y.
v) Figure 13 shows the variation of the effective stresses of coupled analysis along horizontal and vertical axes of the tunnel. It also shows development of pore water pressure. The stresses become asymptotic along horizontal axis at about 5 times the tunnel radius.
vi) The pore water pressure is zero at the tunnel periphery and increases away from it till it equals the pressure due to piezometric head at any point.

4.3.4 Principal stresses

The contours of principal stresses have been plotted in Fig. 14. From the trend of the contours, it can be observed that –

i) Higher concentration of the stresses occurs in the sidewall of the tunnel.
ii) The principal stresses are all compressive in nature.
iii) A relaxation of stresses has been observed at the crown of tunnel.
iv) Principal stresses obtained from coupled stress-flow analysis are less than those obtained from stress analysis (dry condition).
v) The pattern and magnitude of the principal stresses remain similar to that of horizontal and vertical stresses.

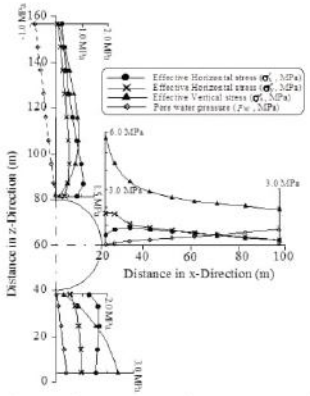

Fig. 13 – Variation of stresses along axes of tunnel mobilized

4.3.5 Effect of various parameters on fluctuation of phreatic surface

An exercise was undertaken to investigate the effect of dip and dip direction of joints in rock mass on the nature of the phreatic surface obtained from coupled stress-flow analysis. Figure 15 shows the fluctuation in the ground water and hence variation in the trend and the level of phreatic surface. The change in trend of phreatic surface is due to:

i) When the dip of the joint changes from 90^O (vertical joint set) to 0° (horizontal joint set), the phreatic surface has been found to rise and it becomes horizontal. It may be due to the smaller permeability in the direction perpendicular to the joint plane as compared to the permeability along the joint plane. Hence, the flow reduces in vertical direction when the joint dip becomes 0°.
ii) The phreatic surface exhibits a totally different behavior for a dip of 45°. A sudden drop in the phreatic surface has been observed above the tunnel crown.
iii) In case when the dip is 45° if the dip direction is changed from 90° to 270°, then a substantial drop in phreatic surface is observed. This behavior is attributed to the direction of flow along the joint plane and towards the tunnel.

iv) The aperture of joint also has a pronounced effect on the phreatic surface. As the joint aperture reduces from 0.50mm to 0.25mm, the phreatic surface rises due to reduction in the permeability of rock joint. As the joint aperture increases, to 1.0mm, the phreatic surface drops down.

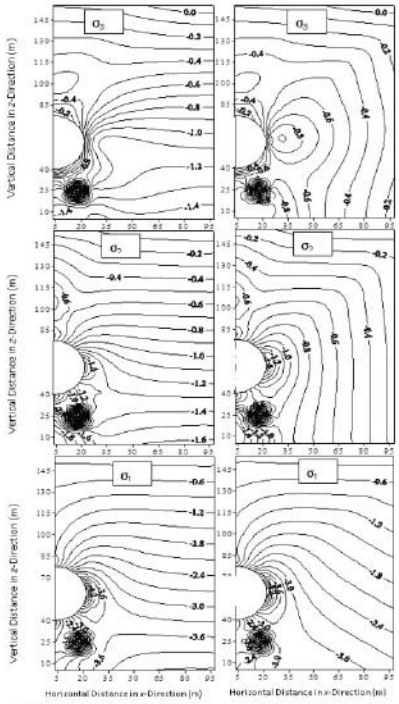

(a) Stress analysis (b) Coupled analysis

Fig. 14 – Contours of principal stresses (MPa) around tunnel

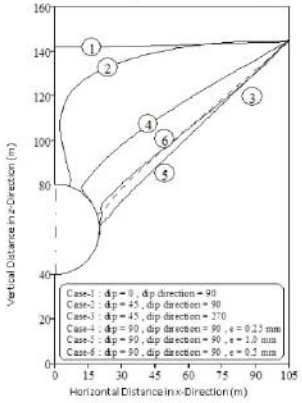

Fig. 15 – Changes in position of phreatic surface with rock mass parameters

5. SUMMARY AND CONCLUSIONS

Many suggestions have been found in the literature to relate the mechanical and hydraulic characteristics of jointed rock mass and various constitutive laws have been proposed. In this study, an attempt has been made to avoid any assumption for constitutive law so as to connect mechanical and hydraulic properties directly.

A case of the tunnel has been investigated to verify the newly derived constitutive laws of coupled stress-flow in jointed rock masses. The results obtained have displayed the capability of the formulation proposed herein to deal with the coupled problem.

The fact remains however that the joints may be considered only as continuous joints. This is one of the limitations of the continuum approach proposed in the present study. The mechanical

properties of the rock material and/or rock joints have significantly altered the behavior. Therefore, choice of such appropriate properties is an important issue for accuracy of the results. The possibility of crushing of asperities of joint surfaces and hence formation of gouge material in the joint spaces causes the closure/obstruction in the flow paths and in turn, alter the hydraulic characteristics of the medium significantly. Therefore, a simulation of the crushing process or creation of new cracks is also essential.

References

Barton, N., Bandis, S. and Bakhtar, K. (1985). Strength, deformation and conductivity coupling of rocks joints, Int. J. Rock Mech. Min. Sci. & Geomech. Abstr., 22(3), pp.121-140.

Barton, C. A., Zoback, M. D., Moos, D. and Sass, J. H. (1995). In-situ stress and fracture permeability in the long valley Caldera, 35th U.S. Symp. on Rock Mechanics, Reno (US), pp.225-229.

Chen, M. and Bai, M. (1998). Modeling stress-dependent permeability of anisotropic fractured porous rocks, Int. J. Rock Mech. & Min. Sci., 35(8), pp.1113-1119.

Elsworth, D. and Goodman, R. E. (1986). Characterization of rock fissure hydraulic conductivity using idealised wall roughness profiles, Int. J. Rock Mech. Min. Sci. & Geomech. Abstr., 23(3), pp.233-244.

Esaki, T., Du, S., Mitani, Y., Ikusada, K. and Jing, L. (1999). Development of a shear-flow test apparatus and determination of coupled properties for a single rock joint, Int. J. Rock Mech. & Min. Sci., 36(5), pp.641-650.

Jing, L. and Hudson, J. A. (2004). Fundamentals of the hydro-mechanical behaviour of rock fractures; roughness characterization and experimental aspects, Int. J. Rock Mech. & Min. Sci., 41(3), Abstract of Paper no. 1A-26, pp.383.

Liao, Q. H. and Hencher, S. R. (1997). Numerical modelling of the hydro-mechanical behavior of fractured rock masses, Int. J. Rock Mech. Min. Sci. & Geomech. Abstr., 34(4/5), Paper No. 177, 428.

Martin, C. D., Davison, C. C. and Kozak, E. T. (1990). Characterizing normal stiffness and hydraulic conductivity of a major shear zone in granite. Int. Symp. on Rock Joints, Loen (Norway), ISRM, pp.549-556.

Olsson, R. and Barton, N. (2001). An improved model for hydromechanical coupling during shearing rock joints, Int. J. Rock Mech. & Min. Sci., 38(3), pp.317-329.

Ouyang, Z. and Elsworth, D. (1993). Evaluation of ground water flow into mined panels, Int. J. Rock Mech. Min. Sci. & Geomech. Abstr., 30(2), pp.71-79.

Rao, K. S. and Gopichand, T. (2002). Analysis and design of underground rock tunnels by boundary element method for Delhi metro project, Indian Geotech. Conf. (IGC-2002), 1, Allahabad (India), pp.513-520.

Wei, L. and Hudson, J. A. (1990). Permeability variation around underground openings in jointed rock masses: A numerical study, Int. Symp. on Rock Joints, Loen (Norway), ISRM, pp.565-569.

Wei, Z. Q. and Hudson, J. A. (1988). Permeability of jointed rock masses. Rock Mech. & Power Plants, ISRM Symp., Madrid (Spain), pp.613-626.

Wang, Y., Wang, Y. and Dai, Y. (2009). Coupling analysis on seepage and stress in jointed rock tunnel with the distinct element method, Computational Structural Engineering, pp.1059–1064.

Amberg, F. (2009). Numerical simulations of tunnelling in soft rock under after pressure, 2nd Int. Conf. on comp. methods in tunneling, Ruhr University Bochum, 9-11 September, Aedificatio Publishers, pp.1- 8.

Prassetyo, S. H. (2017). Hydro-mechanical analysis of tunneling in saturated ground using a novel and efficient sequential coupling technique, Thesis, Department Head Civil and Env. Engg., Univ. of Collarado, boulder, Collarado, USA.

Zhao, C., Zhang, R., Zhang, Q., Shi, Z. and Yu, S. (2018). Shear flow coupled behavior of artificial joints with saw tooth asperities, J. Processes, 6, 152, pp. 1-13.